Russian Technological Journal. 2022;10(5):73–91 ISSN 2500-316X (Online)

UDC 621.3.049.77
https://doi.org/10.32362/2500-316X-2022-10-5-73-91

REVIEW ARTICLE

Technology for the creation of ferroelectric regular domain structures using interfering elastic waves

Vladislav V. Krutov @, Alexander S. Sigov

MIREA – Russian Technological University, Moscow, 119454 Russia
@ Corresponding author, e-mail: v_krutov@mirea.ru

Abstract

Objectives. In many laboratories around the world, work is underway in the field of domain engineering of ferroelectrics. For a number of years, RTU MIREA has been conducting research on the creation of a high-performance technology for the formation of ferroelectric photonic and phononic crystals. The technology is characterized by a short duration of the technological cycle and provides the necessary depth of spatially periodic domain inversion. The key element of the technology is the combined effect of a uniform electric field and interfering high-frequency elastic waves that create a temperature grating. The technology is universal in relation to ferroelectrics of varying degrees of acoustic transparency, which is achieved by using highly dissipative liquid electrodes of a certain thickness. In this case, the energy of elastic waves practically does not penetrate into the ferroelectric, so the manifestation of undesirable effects is excluded. The purpose of this review article is to analyze the results of work carried out at RTU MIREA in the field of technology for the formation of ferroelectric regular domain structures (RDSs) during the period from 2008 to the present.

Methods. Provisions of the theory of propagation, refraction and interference of elastic waves in condensed media are used, in particular, the Newtonian model of a liquid as applied to shear waves, as well as computer simulation. When considering the main stages of the Double Pulse heterothermal technology for the formation of RDSs, methods of analysis and synthesis were applied.

Results. The possibility of forming not only micro-, but also submicron RDSs is shown. Recommendations are given on the choice of the type and specific properties of liquid electrodes, the angles between the direction of propagation of interfering waves, and their frequency. It is shown, in particular, that the use of highly dissipative ionic liquids as liquid electrodes creates favorable conditions for the formation of an RDS with a short period at room temperature. Thus, on shear waves with electrodes based on $LiPF_6$–PC at a frequency of 300 MHz, RDS with a period of about 2 μm can be created. The main technological parameters are determined both for the case of the action of longitudinal elastic waves and for the case of shear waves with horizontal polarization. The results are applicable to ferroelectrics such as lithium niobate, potassium titanyl phosphate, and lead zirconate titanate.

Conclusions. The proposed and studied methods are focused on the mass production of devices based on RDSs, in particular, on the manufacturing of optical parametric oscillators, acoustoelectronic devices, as well as terahertz wave generators and second harmonic oscillators. The technology has a short duration of the technological cycle, comparable to the polarization switching time in the used ferroelectric.

Keywords: domain engineering, ferroelectrics, temperature gratings, double pulse heterothermal technology, elastic waves, acoustic interference method

• **Submitted:** 11.05.2022 • **Revised:** 04.07.2022 • **Accepted:** 12.09.2022

For citation: Krutov V.V., Sigov A.S. Technology for the creation of ferroelectric regular domain structures using interfering elastic waves. *Russ. Technol. J.* 2022;10(5):73–91. https://doi.org/10.32362/2500-316X-2022-10-5-73-91

Financial disclosure: The authors have no a financial or property interest in any material or method mentioned.

The authors declare no conflicts of interest.

ОБЗОРНАЯ СТАТЬЯ

Технология формирования сегнетоэлектрических регулярных доменных структур с использованием интерферирующих упругих волн

В.В. Крутов [@], А.С. Сигов

МИРЭА – Российский технологический университет, Москва, 119454 Россия
[@] Автор для переписки, e-mail: v_krutov@mirea.ru

Резюме

Цели. Работы в области доменной инженерии в сегнетоэлектриках ведутся во многих лабораториях мира. На протяжении ряда лет в РТУ МИРЭА проводятся исследования по созданию высокопроизводительной технологии формирования сегнетоэлектрических фотонных и фононных кристаллов. Технология характеризуется малой продолжительностью технологического цикла и обеспечивает необходимую глубину пространственно-периодического инвертирования доменов. Ключевым звеном технологии является комбинированное воздействие однородного электрического поля и интерферирующих упругих волн высоких частот, создающих температурную решетку. Технология имеет универсальный характер в отношении сегнетоэлектриков различной степени акустической прозрачности, что достигается путем использования сильно диссипативных жидких электродов определенной толщины. При этом энергия упругих волн практически не проникает в сегнетоэлектрик, что исключает проявление нежелательных эффектов. Цель настоящей статьи – анализ результатов работ, выполненных в РТУ МИРЭА, в области технологии формирования сегнетоэлектрических регулярных доменных структур (РДС) в период с 2008 г. по настоящее время.

Методы. Использованы положения теории распространения, преломления и интерференции упругих волн в конденсированных средах, в частности ньютоновская модель жидкости применительно к сдвиговым волнам, а также компьютерное моделирование. При рассмотрении основных этапов биимпульсной гетеротермальной технологии формирования РДС применялись методы анализа и синтеза.

Результаты. Показана возможность формирования не только микро-, но также субмикронных РДС. Даны рекомендации по выбору типа и конкретных свойств жидких электродов, углов между направлением распространения интерферирующих волн, а также их частоты. Показано, что использование в качестве жидких электродов сильно диссипативных ионных жидкостей создает благоприятные условия для формирования РДС с малым периодом при комнатной температуре. Так, на сдвиговых волнах с электродами на основе $LiPF_6$–РС на частоте 300 МГц могут быть созданы РДС с периодом около 2 мкм. Определены основные технологические параметры, как для случая воздействия продольных упругих волн, так и для случая сдвиговых волн с горизонтальной поляризацией. Результаты применимы к таким сегнетоэлектрикам как ниобат лития, титанил-фосфат калия, цирконат-титанат свинца.

Выводы. Предложенные и исследованные методы ориентированы на массовое производство устройств на основе РДС, в т.ч. на изготовление оптических параметрических генераторов, устройств акустоэлектроники, а также генераторов терагерцовых волн и генераторов второй оптической гармоники. Технология обладает малой продолжительностью технологического цикла, сопоставимой с временем переключения поляризации в используемом сегнетоэлектрике.

Ключевые слова: доменная инженерия, сегнетоэлектрики, температурные решетки, биимпульсная гетеротермальная технология, упругие волны, акустоинтерференционный метод

• **Поступила:** 11.05.2022 • **Доработана:** 04.07.2022 • **Принята к опубликованию:** 12.09.2022

Для цитирования: Крутов В.В., Сигов А.С. Технология формирования сегнетоэлектрических регулярных доменных структур с использованием интерферирующих упругих волн. *Russ. Technol. J.* 2022;10(5):73–91. https://doi.org/10.32362/2500-316X-2022-10-5-73-91

Прозрачность финансовой деятельности: Авторы не имеют финансовой заинтересованности в представленных материалах или методах.

Авторы заявляют об отсутствии конфликта интересов.

INTRODUCTION

Methods for creating photonic and phononic crystals based on ferroelectrics and multiferroics have recently been actively studied. Photonic and phononic crystals comprise regular domain structures (RDSs). Figure 1 schematically depicts a ferroelectric RDS of the side-by-side type.

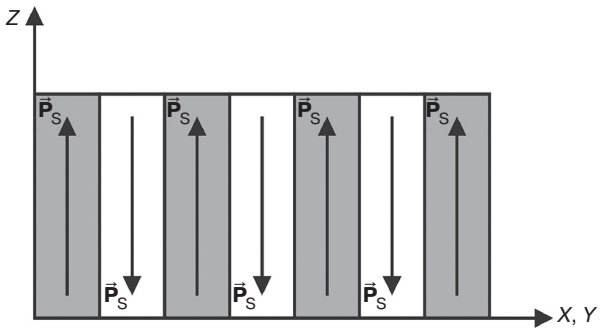

Fig. 1. Side-by-side RDS. Arrows depict the spontaneous polarization vector

Interest in RDSs is mainly due to their capability of performing various functions in acoustoelectronics [1], photonics [2, 3], as well as signal filtering and modulation devices [4, 5].

A number of methods for the creation of RDSs in ferroelectrics have been developed in laboratories around the world over the last 25 years (see, e.g., review [6]). A popular method [3] is based on the use of a nonuniform electric field generated by structured electrodes deposited by photolithography. Methods for "writing a domain pattern" using sequential scanning of the surface of a ferroelectric with a focused laser or electron beam [7] are of little use in the mass production of devices based on RDSs due to their long process cycle and shallow growth of domains. The method [8] based on moving the probe of an atomic force microscope over the ferroelectric surface also involves a long process cycle duration and provides only a shallow domain growth. The method of direct action of interfering laser beams on a single-domain ferroelectric [9] fails to produce a high-quality RDS. The generation of photoinduced charge carriers accompanying laser irradiation leads to undesirable effects such as the destruction of the temperature grating due to heat release by recombining carriers outside the antinodes of the interference pattern. Moreover, birefringence prevents the creation of contrasting temperature grating.

Methods for the creation of RDSs can be considered to be promising if they offer a minimum duration of the process cycle to provide a given depth of growth of domains and high quality RDS.

In recent years, there has been a search for "rapid" industry-oriented methods for the creation of RDSs that do not require the use of photolithography [10–13]. In particular, a method has been demonstrated [10] that allows the creation of surface quasi-periodic domain structures under the action of infrared laser pulses. The main advantage of this method consists in the possibility to produce rapidly domain structures without the use of photolithography. However, the method does not yet allow the creation of periodic domain structures with a given spatial period.

Methods for the creation of RDSs are also studied using a temperature grating induced by interfering elastic waves [13–16]. Such methods are based on the thermal interference principle, according to which local stimulation of domain switching is achieved by the pulsed uniform electric field action and temperature grating created by interfering waves. Figure 2 illustrates a pulsed interfering wave action with power density P and inverting uniform electric field of strength E. The corresponding technology of combined exposure is referred to as double pulse heterothermal (DPH) technology [14]. Selective switching of domains upon application of a uniform electric field is ensured owing to the decreased ferroelectric coercive field with increasing temperature [6]. In comparison with its analogs, this approach reduces the time of the formation of RDSs to values comparable to the polarization switching time of the ferroelectric.

Let us list the main stages of the DPH technology.

1. Creation of an interference pattern using a wave action pulse (creation of a temperature grating).
2. Polarization switching in heated areas of the temperature grating by a uniform electric field with strength $E \geq E_C$, where E_C is the coercive field.
3. Timely switching-off of the electric field upon reaching a given depth of domain growth, as well as in order to prevent lateral growth of domains.

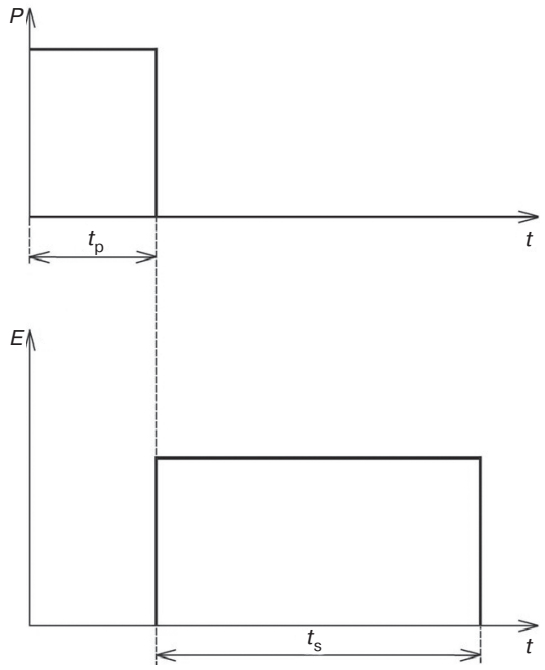

Fig. 2. A pulse of wave action with power density *P* and a pulse of an inverting uniform electric field of strength *E*. t_p is the thermal interference pulse duration, t_s is the duration of uniform electric field exposure

The pulse mode of heterothermal heating is crucial due to the need to prevent the destruction of the temperature grating by heat diffusion.

Since the domain inversion begins at the +*Z*-polar face of a ferroelectric [17, 18], it is expedient to create a temperature grating on the +*Z*-surface of a ferroelectric.

At the same time, in order to induce a contrast temperature grating using interfering waves, it is necessary to take into account the efficiency of the wave absorption in ferroelectrics. In particular, in lithium niobate and tantalate, the absorption is very low over a wide frequency range [19]. Consequently, upon entering a ferroelectric plate, the waves can be repeatedly reflected from its faces, which reduce the contrast of the temperature grating. Therefore, to prevent multiple reflections, it is necessary to create an absorbing layer near the +Z-polar face. In addition, at oblique incidences of ultrasound on the surface of both isotropic and anisotropic solids, birefringence occurs [19–22]. Of course, since the splitting of a refracted wave into longitudinal and transverse waves is highly undesirable when creating a contrasting temperature grating, it preferable that such an absorbing layer as an electrode for applying an inverting voltage be made of an electrically conductive liquid or a metal film. However, the deposition of a metal film is time consuming; moreover, the creation of long-lasting temperature gratings is prevented by the high thermal conductivity of metal materials.

In this article, we consider technology variants based on the use of a temperature grating induced by interfering elastic waves incident on a liquid electrode in contact with the +Z-surface of a ferroelectric (acoustic interference method). The results are applicable to such ferroelectrics as lithium niobate, potassium titanyl phosphate, and lead zirconate titanate.

1. CREATION OF RDSs USING LONGITUDINAL ELASTIC WAVES

1.1. Experimental setup. Calculation of the main parameters. Elastic waves frequency dilemma

Figure 3 shows the working section of the experimental setup intended to create RDSs both in bulk *Z*-cut ferroelectrics and ferroelectric *Z*-oriented films (the electrical circuit was described previously [6]). The operation of the experimental setup is based on the combined effect of two pulses: an interference pulse and an inverting pulse (see INTRODUCTION).

As shown in Fig. 3, an RDS is formed in the region adjacent to the interference pattern in ferroelectric *1* due to the local switching of domains by the uniform electric field using an electrically conductive absorbing liquid film *6* in contact with +*Z*-surface *9* of the ferroelectric. Film *6* functions as an electrode for applying voltage U_c, which performs the local switching of the spontaneous polarization $\vec{\mathbf{P}}_S$ on the temperature grating. The radio pulse U_{AI} is sent to the input of emitters *4* of longitudinal acoustic waves interfering in the area of overlapping beams. In this case, the temperature grating is created on the section of a film *6* that is covered by the interference pattern (the ultrasound absorption coefficient in the liquid film significantly exceeds the absorption in acoustic duct *3*). Due to being in direct contact with the +*Z*-surface, the temperature grating is translated into nucleating layer *8* of the ferroelectric by means of heat transfer. The voltage U_c is applied to both Z-surfaces *9* and *13* for selective reorientation of the domains under the heated areas in the antinodes of the interference pattern. In this case, to transfer the potential from electrode *12* to the −*Z*-surface through liquid *5*, the latter should also be electrically conductive (a "ferroelectric on a solid conductive substrate" variant is also possible).

Acoustic duct *3* of the electroacoustic (EA) module having two emitters *4* is made of a material having a low acoustic wave attenuation coefficient. The components of the circuit are pressed against the ferroelectric crystal through sealing rings *2* (rubber cuffs) using clamp *10*. In order to maintain a constant thickness of liquid film *6* under conditions of possible setup vibrations and ensure the stability of the interference pattern, restrictive protrusions are provided on acoustic block *3*.

Let us consider the algorithm for calculating the process parameters and numerical estimates. When

creating RDSs using the acoustic interference method, the following algorithm can be used for calculating the main process parameters [12]. Here, an RDS is to be created having spatial period d, width b, and length a on the Z-surface. In order to ensure translation of the temperature grating from film *6* to $+Z$-surface *9*, the film thickness must satisfy the condition $\delta << d$. Let, e.g., $\delta \approx d/8$.

Taking into account the damping of the wave according to the Bouguer–Lambert law and assuming that the angles of refraction are small, we choose a film with a thickness approximately equal to the skin depth $1/\alpha$, where α is the absorption coefficient of ultrasound in the film. Then, given that $\delta \approx d/8$, the absorption coefficient is written as

$$\alpha \approx 8/d. \tag{1.1}$$

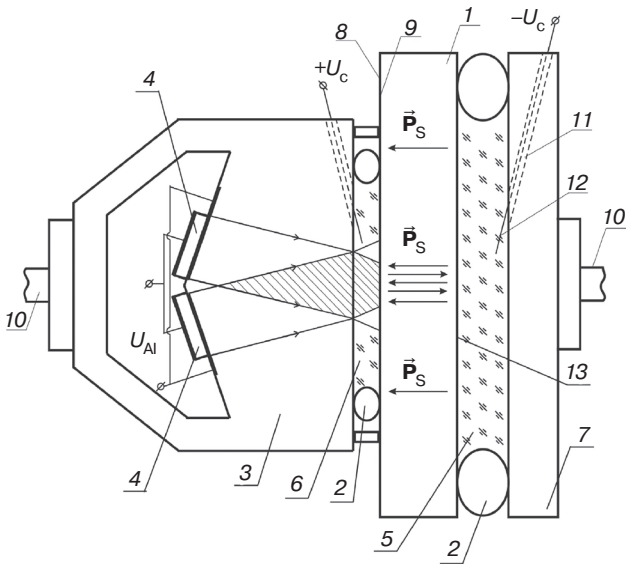

Fig. 3. Part of the setup for creating side-by-side RDSs

According to the Stokes–Kirchhoff formula, the frequency dependence of the absorption coefficient of acoustic waves in a liquid is quadratic: $\alpha = A \cdot f^2$, where A is a coefficient of proportionality. Then, using Eq. (1.1), the required ultrasound frequency is obtained as

$$f \approx \sqrt{8/dA}. \tag{1.2}$$

The period d of the interference pattern created by two beams propagating at an angle of 2β to each other is obtained

$$d = \lambda/(2\sin\beta) \tag{1.3}$$

Then the angle of incidence β of the beams on the absorbing film electrode is estimated at

$$\sin\beta \approx v_S A \cdot f/16, \tag{1.4}$$

where v_S is the speed of ultrasound in the acoustic duct of the EA module.

The aperture length p of each piezoelectric emitter is

$$p \approx a\sqrt{1 - Av_S^2/(32d)}, \tag{1.5}$$

where a is the RDS size (in the direction of the grating vector).

The length L of the acoustic duct of the EA module is found using the formula

$$L \approx \frac{p}{v_S}\sqrt{8d/A}. \tag{1.6}$$

The duration of the interference pulse t_p (for adiabatic heating in the antinodes) should be much less than the relaxation time of the temperature grating and can be estimated at [12]

$$t_p \approx 0.1 \cdot d^2/\chi, \tag{1.7}$$

where χ is the thermal diffusivity of the ferroelectric.

The acoustic pulse power incident on the absorbing film electrode (providing adiabatic heating in the antinodes) is calculated by the expression [23]

$$P_I \approx \frac{\rho_a C_a \chi \Delta T S}{1.6(1-R)d}\left(1 + \frac{8zC\rho}{dC_a\rho_a}\right), \tag{1.8}$$

where C_a, ρ_a, C, and ρ are the specific heat capacity and density of the absorbing film electrode and ferroelectric, respectively; z is the thickness of the nucleating ferroelectric layer; R is the coefficient of reflection from the absorbing film; ΔT is the temperature increment in the temperature grating; and S is the RDS area on the Z-surface.

This expression takes into account the energy consumption for local heating of the absorbing film-electrode and translation of the temperature grating into the nucleating layer of the ferroelectric (by heat transfer).

The pulsed power P_G of the microwave oscillator that is supplied to the input of the piezoelectric emitters is calculated by the formula

$$P_G \approx \frac{P_I \exp(2A_S f^2 L)}{\eta\left[1 - \left(\frac{K_{SW}-1}{K_{SW}+1}\right)^2\right]}, \tag{1.9}$$

where K_{SW} is the standing-wave coefficient in the radio path, η is the efficiency of the conversion of electrical energy into acoustic energy, and A_S is the coefficient of proportionality in the frequency dependence of the absorption coefficient of ultrasound for the material of the acoustic duct [11].

This expression takes into account the loss of acoustic energy in the acoustic duct as well as that due to the conversion of electrical energy into acoustic energy (both the dissipative loss and conversion loss are due to the reflection of the electromagnetic wave from the piezoelectric emitters).

The above expressions were used to calculate the main process parameters of the creation of RDSs in epitaxial *Z*-oriented lead zirconate titanate (PZT) films deposited on a conductive substrate. The RDSs formed in such films are used, e.g., in acoustoelectronics to create acoustic microwave filters [1]. Table 1 presents the results of calculations for an RDS with a width of $b = 25$ μm and a number of periods of $N = 20$ for two spatial period values $d = 0.8$ and 1.2 μm (these values correspond to the RDS created by scanning with an atomic force microscope probe in PZT films having a thickness of 0.2 μm [1]). The material of the liquid absorbing film electrode comprised an aqueous LiCl solution with a low thermal diffusivity ($0.14 \cdot 10^{-6}$ m^2/s), which significantly exceeds the value of this parameter for ferroelectrics. The material of the acoustic duct of the EA module was fused quartz. The following parameter values were used in the calculations [24, 25]: $A \approx 29.9 \cdot 10^{-15}$ s^2/m, $v_S \approx 5.96 \cdot 10^3$ m/s, $A_S \approx 0.015 \cdot 10^{-15}$ s^2/m, $\chi \approx 0.7 \cdot 10^{-6}$ m^2/s, $C = 300$ J $\cdot$ kg$^{-1}\cdot$K^{-1}, $\rho = 7.6 \cdot 10^3$ kg $\cdot$ m^{-3}, $C_a = 3800$ J $\cdot$ kg^{-1} $\cdot$ K^{-1}, $\rho_a = 1.05 \cdot 10^3$ kg $\cdot$ m^{-3}, $R = 0.5$, and $\Delta T = 5$ K.

Table 1 shows that the radio pulse power P_G at the input of the piezoelectric emitters does not exceed 0.1 W. Here it should be noted that the power P_G should not exceed the threshold value to avoid breakdown. This is especially important for gigahertz piezoelectric emitters in which thickness of the piezoelectric layer is quite small. The threshold value of the breakdown power depends on the material of the piezoelectric layer, its thickness, and other parameters, which is the subject of special studies.

From expressions (1.8) and (1.9), it follows that P_G can be reduced, in particular, by decreasing the temperature increment ΔT. Small ΔT values are acceptable in areas with a strong dependence of the coercive field on temperature. As the results of studying PZT showed [26], ΔT can be radically reduced near the Curie point, where the rate of decrease in the coercive field with increasing temperature is maximal.

As follows from expression (1.9), the power P_G can be reduced by decreasing the operating frequency f, the length L, and the absorption coefficient A_S in the acoustic duct of the EA module. In addition, P_G can be reduced by increasing the conversion efficiency η and decreasing the area S, as well as by reducing the reflection loss of the radio pulse from the piezoelectric emitter (by decreasing the standing-wave coefficient K_{SW} using impedance matching).

Expression (1.2) shows that frequency f can be decreased (at a given period d) by increasing the coefficient A of the absorbing film (by choosing appropriate electrolyte solution, solute concentration, and operating temperature).

The relaxation time of the temperature grating is $\tau_d \approx d^2/\chi$. In our calculations, for the period $d \approx 0.8$–1.2 μm, it is $\tau_d \approx 1$–2 μs, i.e., significantly exceeding the duration t_S of the inverting pulse, which for a PZT film is about 50 ns. Therefore, the temperature grating is preserved throughout the inverting pulse. At the same time, the duration of the process cycle (combined exposure to the interference and inverting pulses) is $t_C \approx t_p + t_S \leq 0.25$ μs (Table 1).

Let us estimate the elongation of the sample due to thermal expansion. For PZT, the thermal expansion coefficient is $k \approx 2 \cdot 10^{-6}$ K^{-1} [25]. Then, for a temperature grating having a temperature increment of $\Delta T = 5$ K, the relative elongation is $\Delta a/a \approx k \cdot \Delta T/2 \approx 0.47 \cdot 10^{-5}$. For an RDS with a length of $a \approx 20$ μm (which was used in the calculations), the elongation is $\Delta a \approx 10^{-10}$ m. The obtained value is four orders of magnitude smaller than the RDS periods given in Table 1.

Thus, using the developed model, the main process parameters of the creation of an RDS were estimated as applied to *Z*-oriented PZT films and liquid electrodes based on an aqueous LiCl solution. The calculations showed that, at room temperature (293 K), the creation of an RDS with a period on the order of one micrometer requires interfering elastic waves in the gigahertz range, the generation of which requires very expensive EA modules.

Note that the results of the estimation calculations were obtained for small angles of refraction and under the assumption that the thickness of the liquid electrode layer is approximately equal to the skin depth $\delta \approx d/8$.

As shown previously [27], in order to create an RDS with a small spatial period, including submicron structures, thin ferroelectric samples (i.e., films) should be used due to their specific heat transfer properties.

Table 1. Main process parameters of the creation of RDSs in PZT films

RDS period d, μm	Frequency f, GHz	Pulse duration t_p, μs	Acoustic duct length L, μm	Conversion efficiency η	Standing-wave coefficient K_{SW}	Power at input of liquid electrode P_I, W	Power at input of emitters P_G, W
$d = 1.2$	14.9	0.2	71	0.4	1.3	0.015	0.063
$d = 0.8$	18.3	0.09	38	0.3	1.4	0.019	0.094

The amplitude of the sound pressure of an elastic wave decreases by a factor of e at a distance of 1/α. Formula (1.2) for the carrier frequency of elastic waves was obtained under the assumption of small angles of refraction (for a liquid electrode with a thickness of 1/α). At the same time, after the wave is refracted at the acoustic duct–liquid interface at angle γ, the projection of the distance traveled by the wave onto the normal to the boundary is $\delta_0 = (1/\alpha)\cos\gamma$ ("reduced" skin depth). Earlier [15], for a liquid electrode with a thickness equal to the reduced skin depth, solutions were obtained for the carrier frequency (constructive frequency dilemma) as well as for the angles of refraction. The solutions for the angles of refraction have the form

$$\gamma_1 = \arccos\left(1.15\cos\left(\frac{\pi}{3}+\frac{1}{3}\arccos\frac{Av^2}{12.3d}\right)\right), \quad (1.10)$$

$$\gamma_2 = \arccos\left(1.15\cos\left(\frac{\pi}{3}-\frac{1}{3}\arccos\frac{Av^2}{12.3d}\right)\right), \quad (1.11)$$

where v is the speed of ultrasound in the liquid electrode.

The corresponding solutions for the frequency of interfering waves are given by the formulas

$$f_1 \approx \sqrt{\frac{8\cos\gamma_1}{dA}}, \quad (1.12)$$

$$f_2 \approx \sqrt{\frac{8\cos\gamma_2}{dA}}. \quad (1.13)$$

Based on the results of the modeling, we provided recommendations for choosing the frequency taking into account the state of the art of high-frequency ultrasonic piezoelectric emitters. As can be seen from formulas (1.12) and (1.13), it is advisable when operating at lower frequencies to use liquid electrodes having a high coefficient A value in the frequency dependence $\alpha = Af^2$ of the absorption coefficient of elastic waves.

Note that the values of the "lower" and "upper" frequencies of the elastic waves depend only on the properties of the liquid electrodes and the period of the domain structure.

Thus, the formation of an RDS (with given period d) is possible in two cases:

1) at the lower frequency f_1 with the angle of refraction γ_1 (formulas (1.10) and (1.12)), and
2) at the upper frequency f_2 with the angle of refraction γ_2 (formulas (1.11) and (1.13)).

The obtained results can be used to create similar experimental setups that require one to take into account the state of the art of high-frequency piezoelectric emitters.

1.2. Low-temperature operation

The cost of EA modules is known to sharply increase with increasing operating frequency of the piezoelectric emitter of elastic waves. Keeping in mind the high cost of manufacturing gigahertz piezoelectric emitters, let us consider an economical technological solution involving the use of ultrasonic waves at frequencies close to the lower limit of the microwave range ($f \approx 300$ MHz). As shown below, DPH technology can be used to create RDSs having parameters corresponding to those of the key elements of high-performance acoustoelectronic devices [28], as well as generators and detectors of terahertz radiation [2].

It can be shown that, for a liquid electrode of thickness δ equal to 1/2 of the reduced skin depth, i.e., $\delta = (1/2\alpha)\cos\gamma$, the formulas for the angle of refraction and the frequency f of elastic waves have the form

$$\gamma = \arccos\left(1.154\cos\left(\frac{\pi}{3}-\frac{1}{3}\arccos\frac{Av^2}{6.15d}\right)\right), \quad (1.14)$$

$$f \approx \sqrt{\frac{4\cos\gamma}{dA}}, \quad (1.15)$$

where d is the spatial limit of the RDS.

Solving the system of equations (1.14) and (1.15) gives formulas for the period of the RDS and the coefficient A:

$$d \approx \frac{0.81v}{f}\sqrt{\cos\gamma / \cos(\pi - 3\arccos(0.867\cos\gamma))}, \quad (1.16)$$

$$A \approx \frac{5}{vf}\sqrt{\cos\gamma \cdot \cos(3\arccos(0.867\cos\gamma) - \pi)}. \quad (1.17)$$

The angle of refraction is known to be related to the angle of incidence by Snell's law

$$\gamma = \arcsin\left(\frac{v}{v_S}\sin\beta\right). \quad (1.18)$$

For the phase and group velocities of the elastic wave to have the same direction, the material for the acoustic duct of the EA module should be isotropic. Among isotropic materials, the attenuation of elastic waves is lowest in fused quartz.

Let us consider the operation of an EA module made of fused quartz ($v_S \approx 5.96 \cdot 10^3$ m/s) in combination with a liquid electrode with a speed of ultrasound $v \approx 1.7 \cdot 10^3$ m/s. Previously [16], the frequency dependences of the period d and coefficient A of a liquid electrode were characterized according to expressions (1.16), (1.17), and (1.18).

Figure 4 illustrates the dependences of the period d on the frequency f for three EA modules with β = 10°, 12°, and 17°. For example, at a frequency of $f \approx 300$ MHz and an angle of incidence β ≈ 17°, an RDS with a period of $d \approx 38.0$ μm can be created. RDSs with such a period are used, in particular, in the manufacture of IR optical parametric oscillators [29, 30]. However, to create an RDS with such a period, an appropriate liquid electrode is required. Figure 5 presents the dependence of the coefficient A of the liquid electrode on the frequency f for the same EA modules. It can be seen that, to create an RDS with such a period, a liquid electrode with a very high value of the coefficient $A \approx 1060 \cdot 10^{-15}$ s^2/m is necessary. One of best-studied and most widely available conductive liquids is an aqueous solution of lithium chloride LiCl. However, at a frequency $f \approx 300$ MHz, the coefficient A of a LiCl solution is insufficiently high ($A \leq 550 \cdot 10^{-15}$ s^2/m) even when cooled to $T \approx 223$ K [31]. Therefore, an aqueous LiCl solution is inapplicable for creating an RDS with a period of $d \leq 40$ μm at a frequency close to $f \approx 300$ MHz.

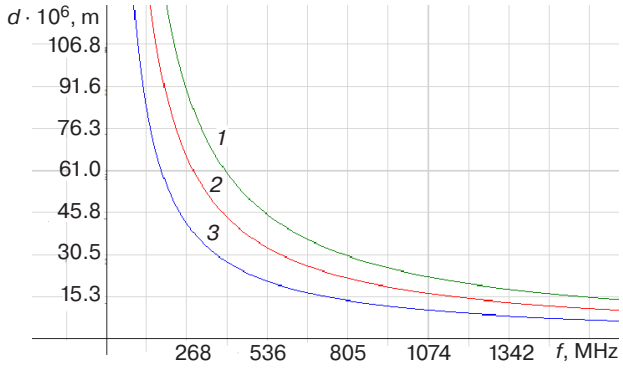

Fig. 4. Period d versus frequency f at three values of the angle of incidence β = (*1*) 10°, (*2*) 12°, and (*3*) 17°

As noted above, RDSs having a period $d \approx 40$–100 μm are the key elements of high-performance acoustic filters [28], as well as generators and detectors of terahertz radiation [2]. The possibility of creating an RDS with such values of the RDS period at a frequency $f \approx 300$ MHz has been demonstrated using a liquid electrode based on a LiCl solution at angles of incidence β < 17° [16]. For example, at β ≈ 10° at a given frequency (as follows from Figs. 4 and 5), the RDS period is $d \approx 80$ μm when using a liquid electrode with $A \approx 230 \cdot 10^{-15}$ s^2/m. This value of the coefficient A can be achieved by cooling the aqueous LiCl solution to a temperature of $T \approx 241$ K [31].

An EA module having a higher frequency $f \approx 670$ MHz has also been modeled [16]. At this frequency and lower temperature of $T \approx 233$ K, the possibility of creating an RDS with a period $d \approx 16$ μm has been demonstrated using a LiCl solution-based liquid electrode [31].

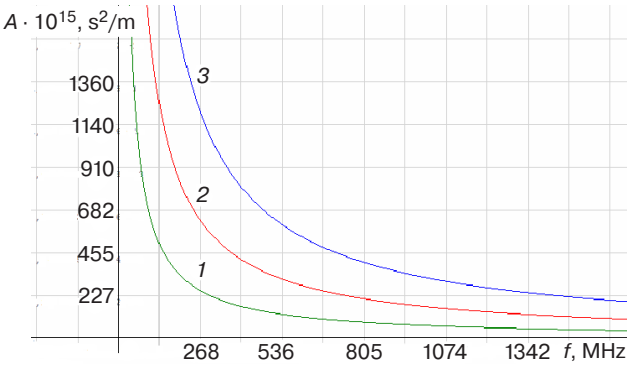

Fig. 5. Coefficient of liquid electrode versus frequency at three values of the angle of incidence β = (*1*) 10°, (*2*) 12°, and (*3*) 17°

In economical terms, EA modules operating at lower frequencies are generally more affordable. For example, domain structures with a period $d \approx 90$ μm can be created at a frequency of $f \approx 270$ MHz and β ≈ 10° using a liquid electrode with $A \approx 250 \cdot 10^{-15}$ s^2/m (e.g., a 7.7 M aqueous LiCl solution at $T \approx 238$ K [31]).

Significantly, RDSs with different periods d can be created using the same EA module (with a specified value of the angle of incidence β) by tuning the frequency within certain limits by means of various liquid electrodes and/or different temperatures.

2. CREATION OF RDSs USING LONGITUDINAL ELASTIC WAVES AND ELECTRODES BASED ON RTIL IONIC LIQUIDS

2.1. Main parameters of some highly dissipative RTIL at room temperature

The possibility of using the acoustic interference method to create RDSs using liquid electrodes based on an aqueous solution of lithium chloride was demonstrated in the previous section. However, the proposed technological solution requires cooling down to temperatures from 233 to 243 K.

In this section, we will discuss the possibility of creating RDSs at room temperature and frequencies near $f \approx 300$ MHz taking into account new data on the acoustic properties of liquid electrodes based on ionic liquids. Salts that melt at room temperature are referred to as room-temperature ionic liquids (RTIL). It will be shown that highly dissipative, electrically conductive RTILs such as 1-butyl-3-methylimidazolium bis(trifluoromethylsulfonyl)imide ([C_4mim][NTf_2]) and 1-hexyl-3-methylimidazolium bis(trifluoromethylsulfonyl)imide ([C_6mim][NTf_2]) create favorable conditions for the formation of RDSs using the acoustic interference method, implementing the technological solution [16] without cooling below

room temperature. The results are applicable to such ferroelectrics as $LiNbO_3$, $KTiOPO_4$, and PZT.

Let us consider the use of RTIL-based liquid electrodes in combination with a fused quartz acoustic duct. The experimental setup for the creation of RDSs using interfering elastic waves was described in section 1.1, as well as in the literature [12]. Figure 6 shows a fragment of this setup: (*1*) ferroelectric, (*2*) acoustic duct of the EA module, (*3*) piezoelectric emitter of longitudinal waves, (*4*) liquid electrode, and (*5*) +*Z*-surface of the ferroelectric. Here, P_S is the spontaneous polarization, β is the angle of incidence on the quartz–liquid interface, γ is the angle of refraction, and P_G is the power at the input of the piezoelectric emitters.

Previously [15], the thickness of the liquid electrode was assumed to be equal to the reduced skin depth $\delta_0 = (1/\alpha)\cos\gamma$. At the same time, in order to reduce the excessively high values of the coefficient *A*, the thickness of the liquid electrode should be selected to be somewhat lower than the reduced skin depth. Since a more significant decrease can lead to a decrease in the contrast of the temperature grating due to the reflection of a significant fraction of the ultrasound energy from the +*Z*-surface of the ferroelectric, this value should be approximately equal to 1/2–3/4 of the reduced skin depth. For example, if the thickness of the liquid electrode is taken to be 1/2 of the reduced skin depth, i.e., $\delta = (1/2\alpha)\cos\gamma$, then the angle of refraction γ, frequency *f*, period *d*, and coefficient *A* can be described by formulas (1.14), (1.15), (1.16), and (1.17), respectively.

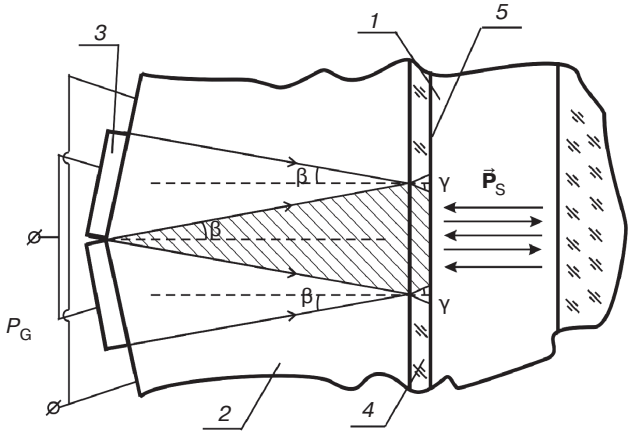

Fig. 6. Fragment of the experimental setup

Table 2 presents some parameters of four RTILs with high values of coefficient *A* at 293 K [32, 33]. It can be seen that these values are more than an order of magnitude higher than those of this coefficient for an aqueous lithium chloride solution at room temperature; as follows from expression (1.15), this allows RDSs to be created at much lower ultrasound frequencies.

Note also that the thermal diffusivity of the RTILs presented in Table 2 is very low (less than half that of water): $\chi \approx 0.6 \cdot 10^{-7}$ m^2/s. This makes it possible to create "long-lived" temperature gratings in RTIL-based liquid electrodes.

2.2. Results of computer modeling of the creation of RDSs at room temperature with ionic liquids

Figure 7 presents the dependence of the coefficient *A* of the liquid electrode on the frequency *f* according to expressions (1.17) and (1.18) for EA modules with angles of incidence β = 17°, 16°, 15°, and 14°. The required value of the coefficient *A* of the liquid electrode can be seen to decrease at a given frequency *f* with decreasing angle of incidence β on the quartz–RTIL interface.

An analysis of the radicands in expressions (1.16) and (1.17) shows that the minimum possible angle of incidence on the quartz–RTIL interface is β ≈ 13° (for liquids with a speed of sound of $v \approx 1260$ m/s). For angles β ≈ 13° and less, there is no real solution. In this case, this angle is independent of the chosen thickness of the liquid electrode, depending only on the v/v_S ratio. At the same time, as follows from Fig. 7, the selection of angles of incidence that significantly exceed β = 17° involves the need to use RTIL with a very high coefficient *A*, which is not always possible at room temperatures [32, 33].

Figure 8 illustrates the dependence of the period *d* on the frequency *f* according to expressions (1.16) and (1.15) for the same EA modules with specified incidence angles β = 17°, 16°, 15°, and 14°. Here, the period *d* of the formed RDS can be seen to increase for an EA module with a specified frequency *f* with decreasing angle of incidence β on the quartz–RTIL interface. Obviously, as follows from Fig. 7, the selection of an excessively low ultrasound frequency results in the need to find an RTIL

Table 2. Parameters of RTILs with high values of the coefficient *A* at an ultrasound frequency of $f \approx 300$ MHz and a temperature of 293 K

RTIL	Coefficient *A*, s^2/m	Speed of ultrasound *v*, m/s	Electrical conductivity σ, S/m	Reference
$[C_2mim][NTf_2]$	$450 \cdot 10^{-15}$	1260	0.9	[32]
$[C_4mim][NTf_2]$	$650 \cdot 10^{-15}$	1260	0.3	[32]
$[C_6mim][NTf_2]$	$800 \cdot 10^{-15}$	1260	0.2	[32]
$[C_4C_1pyr][NTf_2]$	$870 \cdot 10^{-15}$	1260	0.2	[33]

having a rather high value of the coefficient A, which, as noted above, is not always possible at room temperatures.

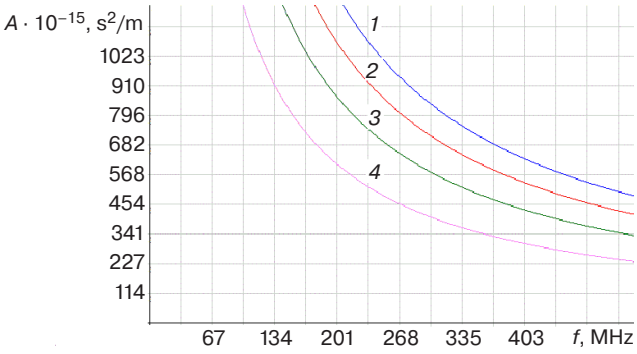

Fig. 7. Coefficient of liquid electrode versus ultrasound frequency at four values of the angle of incidence β = (*1*) 17°, (*2*) 16°, (*3*) 15°, and (*4*) 14°

For example, as follows from Fig. 8, using the EA module operating at a frequency of $f \approx 300$ MHz, at an angle of incidence $\beta \approx 15.5°$, an RDS with a period $d \approx 48$ μm can be created. At the same time, as follows from Fig. 7, to create such an RDS, an appropriate liquid electrode with $A \approx 650 \cdot 10^{-15}$ s²/m is required. As Table 2 shows, the ionic liquid [C_4mim][NTf_2] can be used as such a liquid electrode at a temperature of 293 K (with a conductivity $\sigma \approx 0.3$ S/m). As follows from Figs. 7 and 8, by using another RTIL such as the ionic liquid [C_6mim][NTf_2] (with $A \approx 800 \cdot 10^{-15}$ s²/m at the same temperature) at the same frequency, an RDS can be created having a period $d \approx 42$ μm (with an incidence angle $\beta \approx 16.7°$).

Table 3 presents other examples of creating RDS using RTIL at room temperature. At a frequency $f \approx 300$ MHz with the given RTIL, the spread in values of the angle of incidence β can be seen to comprise approximately 3 degrees.

In practical terms, the most interesting case arises when there is one type of RTIL and one EA module with a specified angle β. In this case, it is possible to create an RDS having a different period d by tuning the ultrasound frequency using the previously characterized [32, 33] temperature dependences of the coefficient A.

The rightmost column of Table 3 presents the estimated durations t_p of an interference pulse calculated for lithium niobate ($\chi \approx 1.54 \cdot 10^{-6}$ m²/s) using formula (1.7). For ferroelectrics having thermal diffusivities lower than that of lithium niobate, such as PZT [34], the corresponding values of the pulse duration t_p are several times longer.

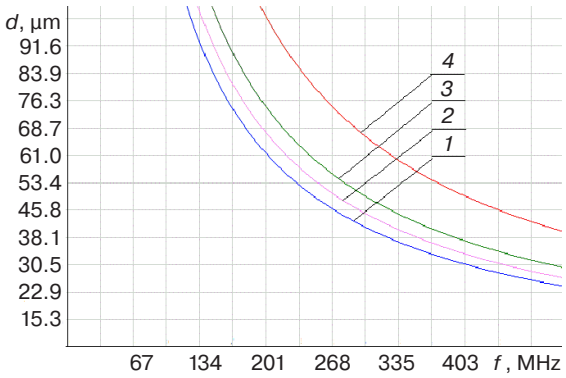

Fig. 8. Period d versus frequency at four values of the angle of incidence β = (*1*) 17°, (*2*) 16°, (*3*) 15°, and (*4*) 14°

The obtained results can be used, e.g., to develop and manufacture high-performance acoustic filters [28], generators of terahertz waves [2], and giant strain actuators [35, 36], especially in their mass production.

3. CREATION OF RDSs USING ELASTIC SHEAR WAVES

3.1. Calculation of the parameters of shear waves and some liquid electrodes in the Newtonian fluid model

In the previous section, we demonstrated the efficacy of using highly dissipative, electrically conductive RTILs as electrodes in the creation of RDSs at room temperature [37]. It is important to note that the use of these liquids opens up more opportunities in terms of choosing the type of elastic waves, since not only longitudinal, but also shear waves can propagate in them. A feature of shear waves is a very small depth of their penetration into the liquid [38]. This feature can significantly increase the efficiency of the technology.

The previously obtained [15] results showed that high values of the coefficient A for liquid electrodes allow the ultrasound frequency to be significantly reduced. Obviously, the use of shear waves can reduce the operating frequency. The use of shear waves can

Table 3. Estimated parameters for the creation of RDSs using ultrasound at a frequency $f \approx 300$ MHz and some RTILs at a temperature of 293 K

RTIL	Coefficient A, s²/m	Angle of incidence β, deg	RDS period d, μm	Pulse duration t_p, μs (for lithium niobate)
[C_2mim][NTf_2]	$450 \cdot 10^{-15}$	14.3	59	226
[C_4mim][NTf_2]	$650 \cdot 10^{-15}$	15.5	48	150
[C_6mim][NTf_2]	$800 \cdot 10^{-15}$	16.7	42	115
[C_4C_1pyr][NTf_2]	$870 \cdot 10^{-15}$	17.2	40	104

also be justified as follows. As is known, reflection and refraction of horizontally polarized shear waves do not result in the splitting of the wave into longitudinal and shear components at any angle of incidence. At the same time, when longitudinal waves are obliquely incident on the interface, the type of the wave is transformed, which may cause significant energy loss.

Whereas there are numerous publications on the use of longitudinal waves in liquids, corresponding studies into the use of shear waves, in particular, horizontally polarized ones, in liquids are not so abundant [39, 40].

As will be shown below, in some conductive liquids, giant values of the coefficient $A \approx (0.482–4.28) \cdot 10^{-10}$ s^2/m were obtained for shear waves at room temperatures. Note that the process of the creation of RDSs using longitudinal waves [37] used ionic liquids with $A \approx (0.2–0.8) \cdot 10^{-12}$ s^2/m (i.e., two orders of magnitude lower).

The experimental setup for the creation of RDS by the acoustic interference method using elastic waves was described in section 1 of this article, as well as in the literature [12, 15]. The setup described in this section differs by virtue of including piezoelectric emitters of shear waves, rather than longitudinal waves.

The wave amplitude decreases by a factor of e at the distance 1/α. For shear waves, 1/α is the depth of penetration of these waves into the liquid, which can be estimated at [38]

$$1/\alpha = \sqrt{\frac{2\eta_0}{\rho\omega}}, \quad (3.1)$$

where η_0 is the viscosity of the liquid at low frequencies, ρ is liquid density, and ω is the circular frequency of the shear waves.

For example, at a viscosity of 0.1 Pas, a density of 1400 kg/m^3, and a frequency f = 200 MHz, the penetration depth 1/α of a shear wave into the liquid is very small (324 nm). The quantity 1/α is also referred to as the skin depth. After the wave is refracted at the acoustic duct–liquid interface at angle γ, the wave amplitude decreases by a factor of e at a distance of 1/α, and the projection of the distance traveled by the wave onto the normal to this interface is $\delta_0 = (1/\alpha)\cos\gamma$ (reduced skin depth).

The velocity of shear waves propagating in a Newtonian fluid ($\omega\tau << 1$, where τ is the shear relaxation time) is described by the formula [40]

$$v \approx \sqrt{2\eta_0\omega/\rho}. \quad (3.2)$$

The coefficient of proportionality A for shear waves in the fluid can be readily found from expression (3.1)

$$A \approx \sqrt{\frac{\pi\rho}{\eta_0 f^3}}. \quad (3.3)$$

Using the condition $\omega\tau << 1$ of the Newtonian fluid model [40] and the values of the shear relaxation times τ of fluids that are given in Table 4, the maximum frequency f_N of shear waves in the model can be estimated at

$$f_N \approx 1/(4\pi\tau). \quad (3.4)$$

Table 4 presents the maximum frequencies f_N of shear waves (in the Newtonian fluid model) as calculated from formula (3.4) and some parameters of fluids used as electrodes: $LiPF_6$–PC electrolyte solution and the ionic liquid 1-butyl-3-methylimidazolium hexafluorophosphate ($[C_4mim][PF_6]$, or [bmim][PF_6]).

For many materials at frequencies above approximately $f \approx 300$ MHz, the elastic waves are significantly attenuated in the acoustic duct of the EA module. To avoid this (other conditions being equal), a higher ultrasound power and more labor-intensive technology has to be used for manufacturing piezoelectric emitters. Based on this, and provided that the condition $f < f_N$ is met for each liquid, the frequencies $f \approx 70$ MHz and $f \approx 300$ MHz were chosen for preliminary estimation of the shear wave velocity v and the coefficient A. Table 5 presents the values of the shear wave velocity v and coefficient A calculated in the Newtonian model using formulas (3.2) and (3.3).

Table 5 shows that, for shear waves, these liquids have giant values of the coefficient $A \approx (0.482–4.28) \cdot 10^{-10}$ s^2/m

Table 4. Values of f_N and parameters of liquid electrodes at room temperature

No.	Liquid	Viscosity η_0, Pa·s	Density ρ, kg/m^3	Relaxation time τ, s	f_N, MHz	Electrical conductivity σ, S/m
1	$LiPF_6$–PC (2 mol/kg)	0.06 [41]	$1.2 \cdot 10^3$ [41]	$0.2 \cdot 10^{-9}$ [42]	400	0.2 [45]
2	$[C_4mim][PF_6]$	0.27 [43]	$1.38 \cdot 10^3$ [43]	$1.1 \cdot 10^{-9}$ [44]	72	0.1 [46]

Table 5. Values of the shear wave velocity v and coefficient A at frequencies not exceeding the maximum frequency f_N of the Newtonian model

No.	Liquid	$f < f_N$, MHz	v, m/s	A, s^2/m
1	$LiPF_6$–PC (2 mol/kg)	300	434.2	$0.482 \cdot 10^{-10}$
2	$[C_4mim][PF_6]$	70	414.9	$2.18 \cdot 10^{-10}$
3	$LiPF_6$–PC (2 mol/kg)	70	209.7	$4.28 \cdot 10^{-10}$

at room temperature. It is also noted that the velocity of the shear waves is several times lower than that of the longitudinal waves.

Taking into account the above limitations, computer modeling was performed to determine the angles of incidence of shear waves on the acoustic duct-liquid interface for given values of the RDS period and develop recommendations for choosing the frequency; the results are discussed in the next section.

3.2. Results of computer modeling for liquid electrodes based on [C_4mim][PF_6] and $LiPF_6$–PC at room temperature

A mathematical model of the effect of interfering elastic waves on a ferroelectric through a liquid layer whose thickness δ is smaller than the RDS half-period ($\delta \approx d/8$) and equal to the reduced skin depth $\delta_0 = (1/\alpha)\cos\gamma$ has been considered earlier[15].

It was determined [15] that, if the condition

$$d \geq 0.081 A v^2, \tag{3.5}$$

is met, then, for a given RDS period, the angle of refraction and the shear wave frequency are described by the expressions

$$\gamma = \arccos\left(1.15\cos\left(\frac{\pi}{3} - \frac{1}{3}\arccos\frac{Av^2}{12.3d}\right)\right), \tag{3.6}$$

$$f \approx \sqrt{\frac{8\cos\gamma}{dA}}. \tag{3.7}$$

We note that the elastic wave velocity v and the coefficient A in formulas (3.6) and (3.7) in the case of shear waves depend on the frequency according to (3.2) and (3.3), respectively.

From expressions (3.6) and (3.7), the following formula for the coefficient is obtained:

$$A \approx \frac{9.92}{vf}\sqrt{\cos\gamma\cos(3\arccos(0.867\cos\gamma) - \pi)}. \tag{3.8}$$

The radicand is nonnegative if $\gamma \geq 0.0475$.

Equating the right-hand sides of expressions (3.3) and (3.8) and taking into account expression (3.2), we obtain the equation for the angle of refraction of shear waves on the acoustic duct–liquid interface:

$$2.4927\cos\gamma\cos(3\arccos(0.867\cos\gamma) - \pi) = 1.$$

Solving this equation gives two values of the angle of refraction:

$$\gamma_1 = 0.455; \gamma_2 = 1.119. \tag{3.9}$$

The angle of refraction γ is known to be related to the angle of incidence β by Snell's law (1.18).

Using expressions (1.18) and (3.2), the frequency dependences of the angles of incidence β on the acoustic duct–liquid interface can be derived:

$$\begin{aligned}\beta_1 &= \arcsin\left(v_S \sin\gamma_1\sqrt{\frac{\rho}{4\pi\eta_0 f}}\right),\\ \beta_2 &= \arcsin\left(v_S \sin\gamma_2\sqrt{\frac{\rho}{4\pi\eta_0 f}}\right).\end{aligned} \tag{3.10}$$

Hence, the conditions follow:

$$v_S \sin\gamma_1\sqrt{\frac{\rho}{4\pi\eta_0 f}} \leq 1,\ v_S \sin\gamma_2\sqrt{\frac{\rho}{4\pi\eta_0 f}} \leq 1. \tag{3.11}$$

Obviously, the case of the smaller angle of incidence β_1 is of the greatest practical interest; since $\gamma_1 = 0.455 < \gamma_2 = 1.119$, this occurs at a lower frequency. In addition, to meet condition (3.11) at lower frequencies, it is advisable to use an EA module made of a material having a low shear wave velocity v_S. Paratellurite α-TeO_2 represents such a material in which the slowest shear sound wave velocity is $v_S = 0.61 \cdot 10^3$ m/s [47]. Then, condition (3.11) for the 2 mol/kg $LiPF_6$–PC liquid is satisfied at $f > f_{min1} \approx 113$ MHz; for the [C_4mim][PF_6] liquid, at $f > f_{min1} \approx 26$ MHz.

Figure 9 illustrates the frequency dependence of the angles of incidence β_1 and β_2 for the 2 mol/kg $LiPF_6$–PC liquid using the EA module based on paratellurite. It can be seen from Fig. 9 that the frequency f_{min2} (for the angles β_2) is approximately equal to 481 MHz for this liquid. In the Newtonian model used here, an RDS can be created at shear wave frequencies simultaneously higher than the frequency f_{min1} and lower than the maximum frequency f_N of the Newtonian model. Therefore, since the condition $f < f_N = 400$ MHz should be satisfied because for the 2 mol/kg $LiPF_6$–PC liquid, only the angles β_1 are of interest.

Similar frequency dependences of the angles of incidence β_1 and β_2 when using the EA module based on paratellurite were also characterized for the [C_4mim][PF_6] liquid. Table 6 presents the minimum frequencies f_{min1} and f_{min2} for these two liquids along with the angles β_1.

It is also necessary to determine the spatial period of the formed RDS. Taking into account expressions (3.3) and (3.7) and two values of the angle of refraction (3.9), we obtain the formulas for the frequency dependence of the RDS period:

$$d_1 = 8\cos\gamma_1 \Big/ \sqrt{\pi\rho f / \eta_0},\ d_2 = 8\cos\gamma_2 \Big/ \sqrt{\pi\rho f / \eta_0}. \tag{3.12}$$

Figure 10 presents the frequency dependences of the RDS period for the 2 mol/kg $LiPF_6$–PC liquid

Table 6. Minimum frequencies, operating frequency range Δf, angle of incidence β_1, and RDS period d_1, calculated for an acoustic duct made of α-TeO_2

No.	Liquid	f_{min1}, MHz	f_{min2}, MHz	Operating frequency range Δf, MHz	Angle of incidence β_1	RDS period d_1, μm	f_N, MHz
1	$[C_4mim][PF_6]$	26	123	30–70	1.410–0.703	10.4–6.8	72
2	$LiPF_6$–PC (2 mol/kg)	113	481	125–400	1.270–0.564	2.6–1.4	400

and the $[C_4mim][PF_6]$ liquid. These dependences can be used to determine the period of the created RDS at frequencies in the range from f_{min1} to f_N. In particular, for the 2 mol/kg $LiPF_6$–PC liquid, at frequencies in the range from f_{min1} = 113 MHz to f_N = 400 MHz; and for the $[C_4mim][PF_6]$ liquid, at frequencies in the range from f_{min1} = 26 MHz to f_N = 72 MHz.

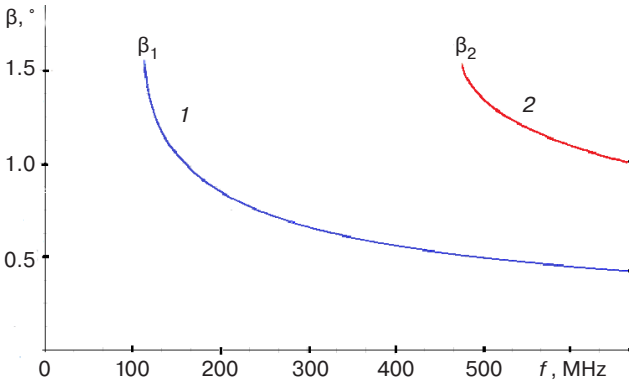

Fig. 9. Frequency dependence of the angles of incidence β_1 and β_2 on the paratellurite–liquid interface for the 2 mol/kg $LiPF_6$–PC liquid

Table 6 presents the results of calculating the minimum frequencies of shear waves, the range Δf of operating frequencies, the angles of incidence β_1, and the RDS period d_1 (for the EA module made of α-TeO_2) for two liquids. Obviously, in practice, the operating frequency range Δf is somewhat smaller than the difference $f_N - f_{min1}$ because the operating frequency is chosen not too close to the frequencies f_{min1} and f_N.

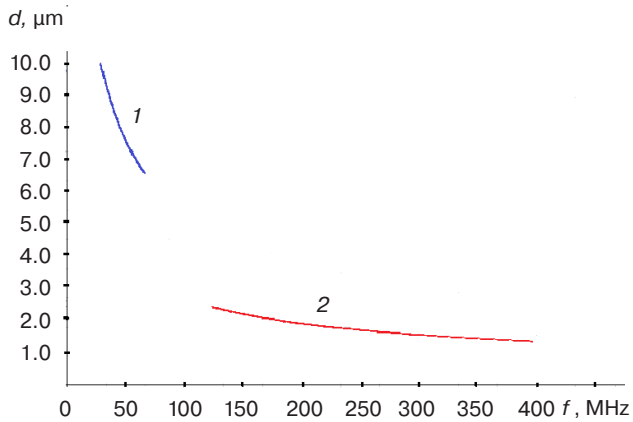

Fig. 10. Frequency dependence of the RDS period for the (*1*) $[C_4mim][PF_6]$ liquid and (*2*) 2 mol/kg $LiPF_6$–PC liquid

From Table 6, it can be seen that the use of a liquid electrode based on the 2 mol/kg $LiPF_6$–PC liquid enables the creation of an RDS with a period of 1.4–2.6 μm at frequencies of 400–125 MHz, respectively.

Thus, by using the acoustic interference method using shear waves, it is possible to create an RDS having a very small spatial period at room temperature with an EA module made of paratellurite, which is a significant advantage over the technology [37] using longitudinal waves.

CONCLUSIONS

The following are the main results obtained at RTU MIREA for the technology used for the creation of ferroelectric RDSs using interfering elastic waves.

1) The proposed technology for creating RDSs uses interfering elastic waves of high and ultrahigh frequencies. In this case, ultrasound is almost completely absorbed in liquid electrodes of a certain thickness and does not penetrate the ferroelectric, which prevents multiple reflections from opposite faces, increases the contrast of the acoustically induced temperature grating, and makes the technology universal (independent of the degree of acoustic transparency of the ferroelectric).
2) It is shown that, when using liquid electrodes based on lithium chloride, the creation of a RDS having a spatial period of several tens of micrometers at ultrasound frequencies of about 300 MHz requires cooling to temperatures of 233 to 243 K. It was also found that, at room temperature, the creation of an RDS requires liquid electrodes for which the coefficient of proportionality in the frequency dependence of the absorption coefficient of ultrasound is an order of magnitude greater than that of a lithium chloride solution.
3) It is shown that the use of such highly dissipative ionic liquids as $[C_4mim][NTf_2]$ and $[C_6mim][NTf_2]$ as liquid electrodes creates favorable conditions for the formation of a short-period RDS at room temperature. Recommendations are given on the choice of the type of ionic liquid, the values of the carrier frequency and pulse duration, as well as the angle of incidence of elastic waves on the fused quartz-liquid interface.

4) Using the Newtonian fluid model, a mathematical model is formulated for the creation of an RDS under the action of interfering shear waves on a ferroelectric through a liquid electrode layer was created. Recommendations are given for selecting the type of the liquid electrode, its thickness, the angle of incidence of shear waves at the paratellurite-liquid interface, as well as the carrier frequency and pulse duration at room temperature. To prevent the splitting of the shear wave at the acoustic duct-liquid interface into two components (longitudinal and shear), it is advisable to use horizontally polarized shear waves.
5) It is shown that shear waves at the same carrier frequency can be used to create an RDS having a spatial period an order of magnitude smaller than that created when using longitudinal waves. For example, whereas the use of longitudinal waves with electrodes based on the $[C_6mim][NTf_2]$ liquid at a frequency of 300 MHz allows an RDS to be created having a period of about 40 μm, shear waves with electrodes based on $LiPF_6$–PC at the same frequency can be used to produce an RDS having a period of about 2 μm.
6) The presented technology combines an extremely short process cycle duration with the necessary depth of domain inversion. In this case, the RDS formation time is comparable to the polarization switching time in the ferroelectric used. The technology can be used in the mass production of devices based on ferroelectric RDSs.

Authors' contribution. All authors equally contributed to the research work.

REFERENCES

1. Sarin Kumar A.K., Paruch P., Marré D., Pellegrino L., Tybell T., Ballandras S., Triscone J.M. A novel high frequency surface acoustic wave device based on piezoelectric interdigital transducers. *Integr. Ferroelectr.* 2004;63(1):55–62. https://doi.org/10.1080/10584580490458621
2. Kitaeva G.K., Kovalev S.P., Naumova I.I., Tuchak A.N., Yakunin P.V., Huang Y.C., Mishina E.D., Sigov A.S. Terahertz wave generation in periodically poled lithium niobate crystals fabricated using two alternative techniques. *Laser Phys. Lett*. 2013;10(5):055404–055409. https://doi.org/10.1088/1612-2011/10/5/055404
3. Yamada M., Nada N., Saitoh M., Watanabe K. First-order quasi-phase matched $LiNbO_3$ waveguide periodically poled by applying an external field for efficient blue second-harmonic generation. *Appl. Phys. Lett*. 1993;629(5):435–437. https://doi.org/10.1063/1.108925
4. Krutov V.V., Shchuka A.A., Mikhalevich V.G. Acoustic dispersive filters and acoustic microwave emitters based on ferroelectrics with spatial modulation of piezoelectric modulus. *Physics of Vibrations*. 2001;9(4):274–279.
5. Esin A.A., Akhmatkhanov A.R., Pavel'ev V.S., Shur V.Ya. Tunable $LiNbO_3$-based diffractive optical element for the control of transverse modes of a laser beam. *Komp'yuternaya optika = Computer Optics*. 2021;45(2):222–226 (in Russ.). https://doi.org/10.18287/2412-6179-CO-786
6. Krutov V.V., Sigov A.S., Shchuka A.A. Techniques for formation of ferroelectric photonic and phononic crystals. *Russ. Technol. J.* 2017;5(2):3–21 (in Russ.). https://doi.org/10.32362/2500-316X-2017-5-2-3-21

СПИСОК ЛИТЕРАТУРЫ

1. Sarin Kumar A.K., Paruch P., Marré D., Pellegrino L., Tybell T., Ballandras S., Triscone J.M. A novel high frequency surface acoustic wave device based on piezoelectric interdigital transducers. *Integr. Ferroelectr.* 2004;63(1):55–62. https://doi.org/10.1080/10584580490458621
2. Kitaeva G.K., Kovalev S.P., Naumova I.I., Tuchak A.N., Yakunin P.V., Huang Y.C., Mishina E.D., Sigov A.S. Terahertz wave generation in periodically poled lithium niobate crystals fabricated using two alternative techniques. *Laser Phys. Lett*. 2013;10(5):055404–055409. https://doi.org/10.1088/1612-2011/10/5/055404
3. Yamada M., Nada N., Saitoh M., Watanabe K. First-order quasi-phase matched $LiNbO_3$ waveguide periodically poled by applying an external field for efficient blue second-harmonic generation. *Appl. Phys. Lett*. 1993;629(5):435–437. https://doi.org/10.1063/1.108925
4. Krutov V.V., Shchuka A.A., Mikhalevich V.G. Acoustic dispersive filters and acoustic microwave emitters based on ferroelectrics with spatial modulation of piezoelectric modulus. *Physics of Vibrations*. 2001;9(4):274–279.
5. Есин А.А., Ахматханов А.Р., Павельев В.С., Шур В.Я. Скоростная модуляция поперечно-модового состава лазерных пучков с помощью дифракционных оптических элементов на основе $LiNbO_3$. *Компьютерная оптика*. 2021;45(2):222–226. https://doi.org/10.18287/2412-6179-CO-786
6. Крутов В.В., Сигов А.С., Щука А.А. Технология создания сегнетоэлектрических фотонных и фононных кристаллов. *Russ. Technol. J.* 2017;5(2):3–21. https://doi.org/10.32362/2500-316X-2017-5-2-3-21

7. Kokhanchik L.S., Irzhak D.V. Formation of regular domain structures and peculiarities of switching of the spontaneous polarization in lithium tantalate crystals during discrete electron irradiation. *Phys. Solid State*. 2010;52(2):306–310. https://doi.org/10.1134/S1063783410020137
[Original Russian Text: Kokhanchik L.S., Irzhak D.V. Formation of regular domain structures and peculiarities of switching of the spontaneous polarization in lithium tantalate crystals during discrete electron irradiation. *Fizika Tverdogo Tela*. 2010;52(2):285–289 (in Russ.).]
8. Volk T., Gainutdinov R., Zhang H. Domain patterning in ion-sliced $LiNbO_3$ films by atomic force microscopy. *Crystals*. 2017;7(5):137–145. https://doi.org/10.3390/cryst7050137
9. Sones C.L., Muir A.C., Ying Y.J., et al. Precision nanoscale domain engineering of lithium niobate via UV laser induced inhibition of poling. *Appl. Phys. Lett.* 2008;92(7):072905-3. https://doi.org/10.1063/1.2884185
10. Shur V.Ya., Mingaliev E.A., Kosobokov M.S., Makaev A.V. Domain structure evolution under multiple pulse heating of lithium niobate by infrared laser. *Ferroelectrics*. 2020;560(1):79–85. https://doi.org/10.1080/00150193.2020.1722886
11. Krutov V.V., Sigov A.S., Shchuka A.A., Kosinov A.A. Technological parameters of the formation of ferroelectric micro- and nanodomain structures by the acoustic interference method. In: *Fundamental Problems of Radioengineering and Device Construction INTERMATIC 2013: Proceedings of the International Scientific and Technical Conference.* 2013. Part 1. P. 139–142.
12. Krutov V.V., Sigov A.S., Shchuka A.A. Quick formation of micro- and nanodomain structures in ferroelectrics by microwave ultrasound interference. *Ferroelectrics*. 2015;476(1):69–74. https://doi.org/10.1080/00150193.2015.998522
13. Krutov V.V., Zasovin E.A., Sigov A.S., Shchuka A.A., Kabin D.V., Mikhalevich V.G. Technology for formation of photonic crystals using UHF elastic wave interference. In: *2008 CriMiCo – 18th International Crimean Conference Microwave and Telecommunication Technology, Conference Proceedings,* Sevastopol, Crimea: 2008; 793–794.
14. Krutov V.V., Zasovin E.A., Mikhalevich V.G., Sigov A.S., Shchuka A.A. Double pulse heterothermal technology for the formation of domain structures in ferroelectrics. *Phys. Solid State*. 2012;54(5):965–967. https://doi.org/10.1134/S1063783412050216
[Original Russian Text: Krutov V.V., Zasovin E.A., Mikhalevich V.G., Sigov A.S., Shchuka A.A. Double pulse heterothermal technology for the formation of domain structures in ferroelectrics. *Fizika Tverdogo Tela.* 2012;54(5):908–910 (in Russ.).]
15. Krutov V.V., Sigov A.S., Shchuka A.A. Phenomenon of formation of regular domain structures in ferroelectrics by uniform electric field and elastic waves: the dilemma of carrier frequencies. *Prikladnaya Fizika = Applied Physics.* 2018;3:53–58 (in Russ.). Available from URL: https://applphys.orion-ir.ru/appl-18/18-3/PF-18-3-53.pdf

7. Коханчик Л.С., Иржак Д.В. Формирование регулярных доменных структур и особенности переключения спонтанной поляризации в кристаллах танталата лития при дискретном облучении электронами. *Физика твердого тела*. 2010;52(2):285–289.
8. Volk T., Gainutdinov R., Zhang H. Domain patterning in ion-sliced $LiNbO_3$ films by atomic force microscopy. *Crystals*. 2017;7(5):137–145. https://doi.org/10.3390/cryst7050137
9. Sones C.L., Muir A.C., Ying Y.J., et al. Precision nanoscale domain engineering of lithium niobate via UV laser induced inhibition of poling. *Appl. Phys. Lett.* 2008;92(7):072905-3. https://doi.org/10.1063/1.2884185
10. Shur V.Ya., Mingaliev E.A., Kosobokov M.S., Makaev A.V. Domain structure evolution under multiple pulse heating of lithium niobate by infrared laser. *Ferroelectrics*. 2020;560(1):79–85. https://doi.org/10.1080/00150193.2020.1722886
11. Крутов В.В., Сигов А.С., Щука А.А., Косинов А.А. Технологические параметры формирования сегнетоэлектрических микро- и нанодоменных структур акустоинтерференционным методом. В сб.: *Фундаментальные проблемы радиоэлектронного приборостроения: материалы Международной научно-технической конференции «INTERMATIC–2013».* 2013. Ч. 1. С. 139–142.
12. Krutov V.V., Sigov A.S., Shchuka A.A. Quick formation of micro- and nanodomain structures in ferroelectrics by microwave ultrasound interference. *Ferroelectrics*. 2015;476(1):69–74. https://doi.org/10.1080/00150193.2015.998522
13. Крутов В.В., Засовин Э.А., Михалевич В.Г., Сигов А.С., Щука А.А., Кабин Д.В. Технология создания фотонных кристаллов с помощью интерференции упругих волн СВЧ диапазона. 18-я Междунар. Крымская конф. «*СВЧ техника и телекоммун. технологии*». Сб. науч. статей. Севастополь, Украина: 8–12 сент. 2008 г. С. 793–794.
14. Крутов В.В., Засовин Э.А., Михалевич В.Г., Сигов А.С., Щука А.А. Биимпульсная гетеротермальная технология формирования доменных структур в сегнетоэлектриках. *Физика твердого тела*. 2012;54(5):908–910.
15. Крутов В.В., Сигов А.С., Щука А.А. Образование регулярных доменных структур в сегнетоэлектриках при воздействии однородного электрического поля и упругих волн: дилемма несущих частот. *Прикладная физика.* 2018;3:53–57. URL: https://applphys.orion-ir.ru/appl-18/18-3/PF-18-3-53.pdf
16. Крутов В.В., Сигов А.С., Щука А.А. Создание сегнетоэлектрических доменных структур с использованием ультразвука вблизи нижней границы СВЧ-диапазона. *Прикладная физика.* 2018;6:60–63. URL: https://applphys.orion-ir.ru/appl-18/18-6/PF-18-6-60.pdf
17. Shur V.Y., Rumyantsev E.L., Batchko R.G., Miller G.D., Fejer M.M., Byer R.L. Domain kinetics in the formation of a periodic domain structure in lithium niobate. *Phys. Solid State*. 1999;41(10):1681–1687. https://doi.org/10.1134/1.1131068
18. Huang L., Jaeger N. Discussion of domain inversion in $LiNbO_3$. *Appl. Phys. Lett.* 1994;65(14):1763–1765. https://doi.org/10.1063/1.112911

16. Krutov V.V., Sigov A.S., Shchuka A.A. Creation of ferroelectric domain structures using ultrasound near the bottom of the UHF band. *Prikladnaya Fizika = Applied Physics*. 2018;6:60–63. Available from URL: https://applphys.orion-ir.ru/appl-18/18-6/PF-18-6-60.pdf
17. Shur V.Y., Rumyantsev E.L., Batchko R.G., Miller G.D., Fejer M.M., Byer R.L. Domain kinetics in the formation of a periodic domain structure in lithium niobate. *Phys. Solid State*. 1999;41(10):1681–1687. https://doi.org/10.1134/1.1131068
18. Huang L., Jaeger N. Discussion of domain inversion in $LiNbO_3$. *Appl. Phys. Lett.* 1994;65(14):1763–1765. https://doi.org/10.1063/1.112911
19. Kaino G. *Akusticheskie volny*. *Ustroistva, vizualizatsiya i analogovaya obrabotka signalov* (*Acoustic waves. Devices, visualization and analog signal processing*). Moscow: Mir; 1990. 652 p. (in Russ.). ISBN 5-03-001434-9
[Kino G.S. *Acoustic waves. Devices, Imaging and Analog Signal Processing.* Prentice-Hall; 1988. 601 p.]
20. Waterman P.C., Teutonico L.J. Ultrasonic double refraction in single crystals. *J. Appl. Phys.* 1957;28(2):266–270. https://doi.org/10.1063/1.1722721
21. Mott G. Reflection and refraction coefficients at a fluid-solid interface. *J. Acoust. Soc. Am*. 1971;50(3B):819–829. https://doi.org/10.1121/1.1912706
22. Ergin K. Energy ratio of the seismic waves reflected and refracted at a rock-water boundary. *Bull. Seismol. Soc. Am*. 1952;42(4):349–372. https://doi.org/10.1785/BSSA0420040349
23. Krutov V.V., Sigov A.S., Shchuka A.A. Acoustic interference method for the formation of micro- and nanodomain structures in ferroelectrics. In: *Metody sozdaniya, issledovaniya mikro-, nanosistem i ekonomicheskie aspekty mikro-, nanoelektroniki: IV Mezhdunarodnaya nauchno-tekhnicheskaya konferentsiya: sbornik statei* (*Methods of Creation, Research of Micro-, Nanosystems and Economic Aspects of Micro-, Nanoelectronics: IV International Scientific and Technical Conference: Collection of Papers*). Penza; 2013. P. 5–8 (in Russ.).
24. Kasper G., Tamm K. Sound propagation at GHz frequencies in aqueous LiCl solutions. *J. Chem. Phys.* 1980;72(9):5279–5289. https://doi.org/10.1063/1.439767
25. Kallaev S.N., Omarov Z.M., Bilalov A.R., Rabadanov M.Kh., Sadykov S.A., Bormanis K. Specific features of the thermal physical properties of relaxor ceramics based on lead zirconate titanate. *Phys. Solid State*. 2009;51(7):1524–1526. https://doi.org/10.1134/S106378340907052X
[Original Russian Text: Kallaev S.N., Omarov Z.M., Bilalov A.R., Rabadanov M.Kh., Sadykov S.A., Bormanis K. Specific features of the thermal physical properties of relaxor ceramics based on lead zirconate titanate. *Fizika Tverdogo Tela*. 2009;51(7):1436–1438 (in Russ.).]
26. Sidorkin A.S., Nesterenko L.P., Ryabtsev S.V., Sidorkin A.A. Frequency dependence of the coercive field and the internal bias field in ferroelectric thin films. *Phys. Solid State*. 2009;51(7):1348–1350. https://doi.org/10.1134/S1063783409070075
19. Кайно Г. *Акустические волны. Устройства, визуализация и аналоговая обработка сигналов.* М.: Мир; 1990. 652 с. ISBN 5-03-001434-9
20. Waterman P.C., Teutonico L.J. Ultrasonic double refraction in single crystals. *J. Appl. Phys.* 1957;28(2):266–270. https://doi.org/10.1063/1.1722721
21. Mott G. Reflection and refraction coefficients at a fluid-solid interface. *J. Acoust. Soc. Am*. 1971;50(3B):819–829. https://doi.org/10.1121/1.1912706
22. Ergin K. Energy ratio of the seismic waves reflected and refracted at a rock-water boundary. *Bull. Seismol. Soc. Am*. 1952;42(4):349–372. https://doi.org/10.1785/BSSA0420040349
23. Крутов В.В., Сигов А.С., Щука А.А. Акустоинтерференционный метод формирования микро- и нанодоменных структур в сегнетоэлектриках. В сб.: *Методы создания, исследования микро-, наносистем и экономические аспекты микро-, наноэлектроники:* IV Международная научно-техническая конференция: сборник статей. Пенза; 2013. С. 5–8.
24. Kasper G., Tamm K. Sound propagation at GHz frequencies in aqueous LiCl solutions. *J. Chem. Phys.* 1980;72(9):5279–5289. https://doi.org/10.1063/1.439767
25. Каллаев С.Н., Омаров З.М., Билалов А.Р., Рабаданов М.Х., Садыков С.А., Борманис К. Особенности теплофизических свойств релаксорной керамики на основе цирконата-титаната свинца. *Физика твердого тела*. 2009;51(7):1436–1438.
26. Сидоркин А.С., Нестеренко Л.П., Рябцев С.В., Сидоркин А.А. Частотная зависимость коэрцитивного поля и внутреннего поля смещения в тонких сегнетоэлектрических пленках. *Физика твердого тела*. 2009;51(7):1277–1279.
27. Крутов В.В., Сигов А.С., Щука А.А. Создание микро- и нанодоменных структур в сегнетоэлектрических пленках с использованием интерферирующего гиперзвука. *Доклады Российской Академии наук. Физика, технические науки*. 2016;469(2):173–176. https://doi.org/10.7868/S0869565216200093
28. Bassignot F., Haye G., Henrot F., Ballandras S., Courjon E., Lesage J.-M. New radio-frequency resonators based on periodically poled lithium niobate thin film and ridge structures. In: *2016. IEEE International Frequency Control Symposium* (*IFCS*). 2016:16302911. https://doi.org/10.1109/FCS.2016.7546793
29. Andreeva M.S., Andreeva N.P., Barashkov M.S., Mitin K.V., Shchebetova N.I., Krymskii M.I., Rogalin V.E., Akhmatkhanov A.R., Chuvakova M.A., Shur V.Ya. Optical parametric oscillator based on the periodically poled MgO:LN crystal with 4.1 μm wavelength and varied pulse duration. *Ferroelectrics*. 2016;496(1):128–134. https://doi.org/10.1080/00150193.2016.1155029
30. Myers L.E., Eckardt R.C., Fejer M.M., Byer R.L., Bosenberg W.R., Pierce J.W. Quasi-phase-matched optical parametric oscillators in bulk periodically poled $LiNbO_3$. *J. Opt. Soc. Am. B*. 1995;12(11):2102–2111. https://doi.org/10.1364/JOSAB.12.002102
31. Kasper G., Tamm K. Sound propagation at GHz frequencies in aqueous LiCl solutions. *J. Chem. Phys*. 1980;72(9):5279–5280. https://doi.org/10.1063/1.439767

[Original Russian Text: Sidorkin A.S., Nesterenko L.P., Ryabtsev S.V., Sidorkin A.A. Frequency dependence of the coercive field and the internal bias field in ferroelectric thin films. *Fizika Tverdogo Tela*. 2009;51(7):1277–11279 (in Russ.).]

27. Krutov V.V., Sigov A.S., Shchuka A.A. Formation of micro-and nanodomain structures in ferroelectric films by interfering hypersound. *Doklady Physics*. 2016;61(7): 332–334. https://doi.org/10.1134/S1028335816070077 [Original Russian Text: Krutov V.V., Sigov A.S., Shchuka A.A. Formation of micro-and nanodomain structures in ferroelectric films by interfering hypersound. *Doklady Akademii Nauk*. 2016;469(2):173–176 (in Russ.). https://doi.org/10.7868/S0869565216200093]
28. Bassignot F., Haye G., Henrot F., Ballandras S., Courjon E., Lesage J.-M. New radio-frequency resonators based on periodically poled lithium niobate thin film and ridge structures. In: *2016. IEEE International Frequency Control Symposium* (*IFCS*). 2016:16302911. https://doi.org/10.1109/FCS.2016.7546793
29. Andreeva M.S., Andreeva N.P., Barashkov M.S., Mitin K.V., Shchebetova N.I., Krymskii M.I., Rogalin V.E., Akhmatkhanov A.R., Chuvakova M.A., Shur V.Ya. Optical parametric oscillator based on the periodically poled MgO:LN crystal with 4.1 μm wavelength and varied pulse duration. *Ferroelectrics*. 2016;496(1):128–134. https://doi.org/10.1080/00150193.2016.1155029
30. Myers L.E., Eckardt R.C., Fejer M.M., Byer R.L., Bosenberg W.R., Pierce J.W. Quasi-phase-matched optical parametric oscillators in bulk periodically poled $LiNbO_3$. *J. Opt. Soc. Am. B*. 1995;12(11):2102–2111. https://doi.org/10.1364/JOSAB.12.002102
31. Kasper G., Tamm K. Sound propagation at GHz frequencies in aqueous LiCl solutions. *J. Chem. Phys*. 1980;72(9):5279–5280.https://doi.org/10.1063/1.439767
32. Zorębski M., Zorębski E., Dzida M., Skowronek J., Jężak S., Goodrich P., Jacquemin J. Ultrasonic relaxation study of 1-alkyl-3-methylimidazolium-based room-temperature ionic liquids: probing the role of alkyl chain length in the cation. *J. Phys. Chem. B*. 2016;120(14): 3569–3581. https://doi.org/10.1021/acs.jpcb.5b12635
33. Zorębski E., Zorębski M., Musiał M., Dzida M. Ultrasonic relaxation spectra for pyrrolidinium bis(trifluoromethylsulfonyl)imides: A comparison with imidazolium bis(trifluoromethylsulfonyl)imides. *J. Phys. Chem. B*. 2017;121(42):9886–9894. https://doi.org/10.1021/acs.jpcb.7b07433
34. Malyshkina O.V., Movchikova A.A., Kalugina O.N., Daineko A.V. Determination of thermal diffusivity coefficient of thin films by thermal square wave method. *Ferroelectrics*. 2011;424(1):28–35. https://doi.org/10.1080/00150193.2011.623637
35. Li F., Wang Q., Miao H. Giant actuation strain nearly 0.6% in a periodically orthogonal poled lead titanate zirconate ceramic *via* reversible domain switching. *J. Appl. Phys.* 2017;122(7):074103–074109. https://doi.org/10.1063/1.4997940
36. Wang Q., Li F. A low-working-field (2 kV/mm), large-strain (>0.5%) piezoelectric multilayer actuator based on periodically orthogonal poled PZT ceramics. *Sensors and Actuators A: Physical*. 2018;272:212–219. https://doi.org/10.1016/j.sna.2018.01.042

32. Zorębski M., Zorębski E., Dzida M., Skowronek J., Jężak S., Goodrich P., Jacquemin J. Ultrasonic relaxation study of 1-alkyl-3-methylimidazolium-based room-temperature ionic liquids: probing the role of alkyl chain length in the cation. *J. Phys. Chem. B*. 2016;120(14): 3569–3581. https://doi.org/10.1021/acs.jpcb.5b12635
33. Zorębski E., Zorębski M., Musiał M., Dzida M. Ultrasonic relaxation spectra for pyrrolidinium bis(trifluoromethylsulfonyl)imides: A comparison with imidazolium bis(trifluoromethylsulfonyl)imides. *J. Phys. Chem. B*. 2017;121(42):9886–9894. https://doi.org/10.1021/acs.jpcb.7b07433
34. Malyshkina O.V., Movchikova A.A., Kalugina O.N., Daineko A.V. Determination of thermal diffusivity coefficient of thin films by thermal square wave method. *Ferroelectrics*. 2011;424(1):28–35. https://doi.org/10.1080/00150193.2011.623637
35. Li F., Wang Q., Miao H. Giant actuation strain nearly 0.6% in a periodically orthogonal poled lead titanate zirconate ceramic *via* reversible domain switching. *J. Appl. Phys.* 2017;122(7):074103–074109. https://doi.org/10.1063/1.4997940
36. Wang Q., Li F. A low-working-field (2 kV/mm), large-strain (>0.5%) piezoelectric multilayer actuator based on periodically orthogonal poled PZT ceramics. *Sensors and Actuators A: Physical*. 2018;272:212–219. https://doi.org/10.1016/j.sna.2018.01.042

37. Krutov V.V., Sigov A.S., Shchuka A.A. A technique for the formation of ferroelectric regular domain structures using highly dissipative electrically conductive liquids at room temperature. *Ferroelectrics*. 2020;559(1):120–127. https://doi.org/10.1080/00150193.2020.1722013
38. Landau L.D., Lifshitz E.M. *Fluid Mechanics*. London: Pergamon Press; 1959. § 24.
39. Greenwood M.S., Bamberger J.A. Measurement of viscosity and shear wave velocity of a liquid or slurry for on-line process control. *Ultrasonics*. 2002;39(9):623–630. https://doi.org/10.1016/S0041-624X(02)00372-4
40. Kielczyński P., Pajewski W. Transmission of SH plane waves obliquely incident at a plane interface between an elastic solid and a viscoelastic liquid. *Acta Acust. United Acust*. 1990;71(1):21–27.
41. Yamaguchi T., Yonezawa T., Yoshida K., Yamaguchi T., Nagao M., Faraone A., Seki S. Relationship between structural relaxation, shear viscosity, and ionic conduction of $LiPF_6$/propylene carbonate solutions. *J. Phys. Chem. B*. 2015;119(51):15675–15682. https://doi.org/10.1021/acs.jpcb.5b08701
42. Yamaguchi T., Yoshida K., Yamaguchi T., Nagao M., Faraone A., Seki S. Decoupling between the temperature-dependent structural relaxation and shear viscosity of concentrated lithium electrolyte. *J. Phys. Chem. B*. 2017;121(37):8767–8773. https://doi.org/10.1021/acs.jpcb.7b04633
43. Yamaguchi T., Miyake S., Koda S. Shear relaxation of imidazolium-based room-temperature ionic liquids. *J. Phys. Chem. B*. 2010;114(24):8126–8133. https://doi.org/10.1021/jp1024137
44. Yamaguchi T., Nakahara E., Koda S. Quantitative analysis of conductivity and viscosity of ionic liquids in terms of their relaxation times. *J. Phys. Chem. B*. 2014;118(21):5752–5759. https://doi.org/10.1021/jp502631q

37. Krutov V.V., Sigov A.S., Shchuka A.A. A technique for the formation of ferroelectric regular domain structures using highly dissipative electrically conductive liquids at room temperature. *Ferroelectrics*. 2020;559:1:120–127. https://doi.org/10.1080/00150193.2020.1722013
38. Landau L.D., Lifshitz E.M. *Fluid Mechanics.* London: Pergamon Press; 1959. § 24.
39. Greenwood M.S., Bamberger J.A. Measurement of viscosity and shear wave velocity of a liquid or slurry for on-line process control. *Ultrasonics*. 2002;39(9):623–630. https://doi.org/10.1016/S0041-624X(02)00372-4
40. Kielczyński P., Pajewski W. Transmission of SH plane waves obliquely incident at a plane interface between an elastic solid and a viscoelastic liquid. *Acta Acust. United Acust*. 1990;71(1):21–27.
41. Yamaguchi T., Yonezawa T., Yoshida K., Yamaguchi T., Nagao M., Faraone A., Seki S. Relationship between structural relaxation, shear viscosity, and ionic conduction of $LiPF_6$/propylene carbonate solutions. *J. Phys. Chem. B*. 2015;119(51):15675–15682. https://doi.org/10.1021/acs.jpcb.5b08701
42. Yamaguchi T., Yoshida K., Yamaguchi T., Nagao M., Faraone A., Seki S. Decoupling between the temperature-dependent structural relaxation and shear viscosity of concentrated lithium electrolyte. *J. Phys. Chem. B*. 2017;121(37):8767–8773. https://doi.org/10.1021/acs.jpcb.7b04633
43. Yamaguchi T., Miyake S., Koda S. Shear relaxation of imidazolium-based room-temperature ionic liquids. *J. Phys. Chem. B*. 2010;114(24):8126–8133. https://doi.org/10.1021/jp1024137
44. Yamaguchi T., Nakahara E., Koda S. Quantitative analysis of conductivity and viscosity of ionic liquids in terms of their relaxation times. *J. Phys. Chem. B*. 2014;118(21):5752–5759. https://doi.org/10.1021/jp502631q
45. Kondo K., Sano M., Hiwara A., Omi T., Fujita M., Kuwae A., Yokoyama H. Conductivity and solvation of Li^+ ions of $LiPF_6$ in propylene carbonate solutions. *J. Phys. Chem. B*. 2000;104(20):5040–5044. https://doi.org/10.1021/jp000142f
46. Umecky T., Kanakubo M., Makino T., Aizawa T., Suzuki A. Effect of CO_2 dissolution on electrical conductivity and self-diffusion coefficients of 1-butyl-3-methylimidazolium hexafluorophosphate ionic liquid. *Fluid Phase Equilib*. 2013;357:76–79. https://doi.org/10.1016/j.fluid.2013.05.023
47. Ohmachi Y., Uchida N. Temperature dependence of elastic, dielectric, and piezoelectric constants in TeO_2 single crystals. *J. Appl. Phys*. 1970;41(6):2307–2311. https://doi.org/10.1063/1.1659223

45. Kondo K., Sano M., Hiwara A., Omi T., Fujita M., Kuwae A., Yokoyama H. Conductivity and solvation of Li^+ ions of $LiPF_6$ in propylene carbonate solutions. *J. Phys. Chem. B*. 2000;104(20):5040–5044. https://doi.org/10.1021/jp000142f
46. Umecky T., Kanakubo M., Makino T., Aizawa T., Suzuki A. Effect of CO_2 dissolution on electrical conductivity and self-diffusion coefficients of 1-butyl-3-methylimidazolium hexafluorophosphate ionic liquid. *Fluid Phase Equilib*. 2013;357:76–79. https://doi.org/10.1016/j.fluid.2013.05.023
47. Ohmachi Y., Uchida N. Temperature dependence of elastic, dielectric, and piezoelectric constants in TeO_2 single crystals. *J. Appl. Phys*. 1970;41(6):2307–2311. https://doi.org/10.1063/1.1659223

About the authors

Vladislav V. Krutov, Cand. Sci. (Eng.), Associate Professor, Department of Nanoelectronics, Institute for Advanced Technologies and Industrial Programming, MIREA – Russian Technological University (78, Vernadskogo pr., Moscow, 119454 Russia). E-mail: v_krutov@mirea.ru. https://orcid.org/0000-0003-1909-1435

Alexander S. Sigov, Academician at the Russian Academy of Sciences, Dr. Sci. (Phys.-Math.), Professor, President, MIREA – Russian Technological University (78, Vernadskogo pr., Moscow, 119454 Russia). E-mail: sigov@mirea.ru. ResearcherID L-4103-2017, Scopus Author ID 35557510600, RSCI SPIN-code 2869-5663, https://www.researchgate.net/profile/A_Sigov

Об авторах

Крутов Владислав Викторович, к.т.н., доцент, кафедра наноэлектроники Института перспективных технологий и индустриального программирования, ФГБОУ ВО «МИРЭА – Российский технологический университет» (119454, Россия, Москва, пр-т Вернадского, д. 78). E-mail: v_krutov@mirea.ru. https://orcid.org/0000-0003-1909-1435

Сигов Александр Сергеевич, академик РАН, д.ф.-м.н., профессор, президент ФГБОУ ВО «МИРЭА – Российский технологический университет» (119454, Россия, Москва, пр-т Вернадского, д. 78). E-mail: sigov@mirea.ru. ResearcherID L-4103-2017, Scopus Author ID 35557510600, SPIN-код РИНЦ 2869-5663, https://www.researchgate.net/profile/A_Sigov

Translated from Russian into English by Vladislav V. Glyanchenko
Edited for English language and spelling by Thomas A. Beavitt